J. Fluid Mech. (1983), *vol.* 135, *pp.* 235–259
Printed in Great Britain

Onset of Rayleigh–Bénard convection in binary liquid mixtures of ^{3}He in ^{4}He

By G. W. T. LEE†, P. LUCAS AND A. TYLER
Schuster Laboratory, Department of Physics, University of Manchester, Manchester M13 9PL

(Received 26 July 1982 and in revised form 18 July 1983)

We describe experiments in which we have observed the onset of Rayleigh–Bénard convection in normal liquid ^{3}He–^{4}He mixtures. Evidence of overstability was seen when heating from below but only stationary convection was observed when heating from above. Measurements of the critical Rayleigh number are presented and compared with the predictions of current theories of marginal stability in a binary mixture. These experiments exemplify liquid ^{3}He–^{4}He mixtures as a system for the study of convective instabilities.

1. Introduction

The problem of Rayleigh–Bénard (RB) convection in a two-component fluid system has attracted a steady interest for many years, as can be seen from the reviews by Schechter, Velarde & Platten (1974) and Gershuni & Zhukovitskii (1976). An interesting early experimental study is that of Caldwell (1970). The problem is more complex than that of the one-component fluid because a gradient in the relative concentration of the two components can contribute to a density gradient just as effectively as can a temperature gradient. Furthermore, the presence of two diffusive modes allows either stationary or overstable flow states at the onset of convection depending on the magnitude of the fluid parameters, the boundary conditions and the competition between thermal expansion and thermal diffusion.

Above its superfluid transition temperature T_λ (0.867 K $< T_\lambda <$ 2.172 K, depending on concentration), a ^{3}He–^{4}He liquid mixture is termed normal since it behaves in every way like a classical binary fluid mixture. Close to T_λ a normal mixture is a particularly interesting experimental system for testing theoretical ideas on RB convection. Such a mixture obeys exactly the same hydrodynamics as do the organic fluid mixtures and ionic salt solution mixtures so far investigated, even having fluid parameters D, D_T, k_T and β_T of roughly similar magnitudes provided the mixture temperature is of the order of 10^{-2} K or more above T_λ. Here D is the mass-diffusion coefficient, D_T the thermal diffusivity, k_T the thermal-diffusion ratio and β_T the thermal-expansion coefficient.

Close to but above T_λ, however, where the normal mixture still obeys the standard hydrodynamics, the ratio D/D_T diverges approximately as $(T-T_\lambda)^{-\frac{1}{2}}$, k_T limits to about 0.6 in the zero-concentration limit, and β_T, which is positive well above T_λ, falls to zero about 7 mK above T_λ, and then as T_λ is approached becomes large and negative. These properties, particularly the last, allow the experimenter great freedom in varying the fluid parameter values and the extent of the competition between thermal expansion and thermal diffusion simply by adjusting the mean concentration and temperature of the mixture. This feature of ^{3}He–^{4}He mixtures is

† Present address: VG Analytical Ltd, Altrincham, Cheshire WA14 5REZ.

quite unique amongst binary fluid systems, and allows the exploration of an extremely wide range of the dimensionless parameters necessary for a description of RB convection.

Although not the subject of this report, it is worth remarking that below the λ-point the superfluid mixture is equally interesting in that it can display features of a one-component system with a Prandtl number of order 0.1 despite a non-zero normal component velocity below the onset of convection (Warkentin *et al.* 1980; Haucke *et al.* 1981; Fetter 1981), and may possess two types of oscillatory instability (Steinberg 1981*b*). Also, when a mixture of molar ^{3}He concentration 0.675 (X_t) is cooled to 0.867 K (T_t), it simultaneously experiences the superfluid transition and phase separation. In the phase diagram of concentration and temperature this is called the tricritical point. At this point more unusual convective features can be expected (Steinberg 1981*a*, *b*), since k_T diverges as $(T-T_t)^{-1}$ and D vanishes.

Whilst the use of cryogenic fluids for these investigations may appear unnecessary in view of the abundance of room-temperature mixtures which are available, low-temperature systems offer the advantages of good thermal isolation, precision thermometry and short thermal response times, as summarized by Ahlers (1975).

In this report we confine ourselves to normal ^{3}He–^{4}He mixtures near the λ-line. In §2 the current status of the linear theory of convection in non-superfluid binary mixtures is reviewed. In §3 we present our experimental results on the onset of convection in these mixtures. Section 4 is concerned with the reduction of the data to dimensionless form for comparison with theory, and in §5 we make some concluding remarks.

2. Theory

2.1. *Nomenclature of binary-mixture models*

The equations of mass and heat transport together with the mass and conservation equations are (Landau & Lifshitz 1959; De Groot & Mazur 1962; Gershuni & Zhukovitskii 1976)

$$\boldsymbol{i} = -\rho D\boldsymbol{\nabla}c - \frac{\rho D k_T}{T}\boldsymbol{\nabla}T, \tag{1}$$

$$\boldsymbol{q}' = \kappa\boldsymbol{\nabla}T + k_T\left(\frac{\partial \Delta}{\partial c}\right)_{T,P}\boldsymbol{i}, \tag{2}$$

$$\rho C_p\left(\boldsymbol{u}\cdot\boldsymbol{\nabla} + \frac{\partial}{\partial t}\right)T = -\boldsymbol{\nabla}\cdot\boldsymbol{q}', \tag{3}$$

$$\rho\left(\boldsymbol{u}\cdot\boldsymbol{\nabla} + \frac{\partial}{\partial t}\right)c = -\boldsymbol{\nabla}\cdot\boldsymbol{i}. \tag{4}$$

The above notation is that of Landau & Lifshitz (1959). From here on these equations will be discussed as for a normal ^{3}He–^{4}He mixture, but they are valid for any classical binary mixture. In these equations $\boldsymbol{i}$ is the diffusion mass flux of one species, chosen to be ^{3}He, and $\boldsymbol{q}'$ is the heat flux with the heat convected by the two diffusion fluxes subtracted off. The ^{3}He component has mass concentration c and molar concentration X, mass-diffusion coefficient D and thermal-diffusion ratio k_T, and the mixture has density ρ, thermal conductivity κ (measured under conditions where $\boldsymbol{i} = 0$), specific heat per unit mass at constant pressure C_p, fluid velocity $\boldsymbol{u}(\boldsymbol{r}, t)$, and is at temperature T and pressure P. The quantity Δ equals $\mu_3 - \mu_4$, where

$m_3\mu_3 = (\partial g/\partial n_3)_{T,P}$ and $m_4\mu_4 = (\partial g/\partial n_4)_{T,P}$ define the respective partial chemical potentials of the ^{3}He and ^{4}He in solution, and m_3 and m_4 are the atomic masses. The Gibbs free energy of the solution and the numbers n_3 and n_4 of atoms of ^{3}He and ^{4}He respectively refer to 1 g of solution.

The configuration of the Bénard cell is as follows: the fluid mixture is confined between two horizontal plates spaced distance d apart in the z-direction and, at least in an idealized geometry, unbounded in the lateral x- and y-directions. Such a geometry has infinite aspect ratio.

Combining (1)–(4) and introducing the Navier–Stokes equation in the Boussinesq approximation yields three coupled equations which determine the evolution of the system:

$$\left(\boldsymbol{u}\cdot\boldsymbol{\nabla}+\frac{\partial}{\partial t}\right)c = D\nabla^2 c + \frac{Dk_T}{T}\nabla^2 T, \tag{5}$$

$$\left(\boldsymbol{u}\cdot\boldsymbol{\nabla}+\frac{\partial}{\partial t}\right)T = (D_T + AD)\nabla^2 T + \frac{ATD}{k_T}\nabla^2 c, \tag{6}$$

$$\left(\boldsymbol{u}\cdot\boldsymbol{\nabla}+\frac{\partial}{\partial t}\right)\boldsymbol{u} = -\frac{1}{\rho_L}\boldsymbol{\nabla}P - \frac{\rho}{\rho_L}g\boldsymbol{i}_z + \nu\nabla^2\boldsymbol{u}. \tag{7}$$

Here ρ_L is the fluid density at the lower cell plate, g is the magnitude of the acceleration due to gravity, and ν is the fluid kinematic viscosity. The dimensionless quantity A is equal to $k_T^2(\partial\Delta/\partial C)_{T,P}/TC_p$. In the approximation that the propagating sound mode is neglected, the fluid is incompressible so that div $u = 0$. $\boldsymbol{i}_z$ is a unit vector pointing vertically upward in the z-direction.

The set of equations (5)–(7) describe a 'double-diffusive' fluid system in that it possesses two diffusive modes. However, this term is usually reserved for the special case $k_T = 0$, when the fluid system then corresponds to that studied by, for example, Nield (1967), Huppert & Moore (1976) and Da Costa, Knobloch & Weiss (1981), who refer to the ensuing convection as 'thermohaline', 'double-diffusive' and 'thermosolutal' respectively.

A considerable body of literature on Bénard convection exists for the case where the Soret term $(\rho Dk_T/T)\,\boldsymbol{\nabla}T$ in (1) is retained but the Dufour term $k_T(\partial\Delta/\partial c)_{T,P}\boldsymbol{i}$ in (2) is omitted as negligible – for example Hurle & Jakeman (1971), where the system is termed 'Soret-driven thermosolutal', Schechter, Prigogine & Hamm (1972) and the review article by Schechter, Velarde & Platten (1974). This case corresponds to setting $A = 0$ in the set of equations (5)–(7).

Only recently has convection been examined where both Soret and Dufour terms are retained (Gershuni & Zhukovitskii 1976; Lee *et al.* 1978; Lee, Lucas & Tyler 1979; Gutkowicz-Krusin, Collins & Ross 1979*a*, *b*; Knobloch 1980), and, following this last author, it would seem reasonable to term this case the 'Soret–Dufour' problem, to which we confine ourselves in the remainder of this report. We note that Gutkowicz-Krusin *et al.* (1979*a*) are in error in omitting the term $AD\nabla^2 T$ in their version of our equation (6). The Soret–Dufour problem is the most general, with no approximation being made *a priori* regarding the relative magnitudes of thermal coefficients. This is the model most appropriate to liquid ^{3}He–^{4}He mixtures because the large size of k_T near the lambda and tricritical regions of the (c, T) plane ensures that neither the Soret nor the Dufour contribution can be neglected. This is demonstrated in table 1, which includes the current state of our knowledge on the parameters k_T and A at a representative set of values of $T - T_\lambda$.

$T-T_\lambda$ (mK)	k_T	β_T (K^{-1})	$(\partial A/\partial c)_{T,P}$ (10^2 J mol^{-1})	D (10^{-6} cm^2 s^{-1})	ν (10^{-4} cm^2 s^{-1})	D_T (10^{-4} cm^2 s^{-1})	A	Pr	Sc'	S	H
					$X = 0.016$						
1	2.36×10^{-1}	-1.54×10^{-2}	18.4	51.6	1.69	3.00	1.46	0.564	1.33	4.43	1.93
4	9.02×10^{-2}	-5.11×10^{-3}	18.0	29.7	1.70	2.74	2.68×10^{-1}	0.622	4.51	5.09	6.09
10	3.17×10^{-2}	2.33×10^{-3}	17.7	20.6	1.73	2.74	3.99×10^{-2}	0.631	8.08	−3.90	17.2
40	2.79×10^{-3}	1.46×10^{-2}	17.2	11.9	1.82	3.05	4.23×10^{-4}	0.598	15.3	-5.43×10^{-2}	−1.47
100	2.83×10^{-4}	2.33×10^{-2}	16.8	8.23	1.94	3.45	5.22×10^{-6}	0.561	23.6	-3.35×10^{-3}	−0.141
					$X = 0.079$						
1	2.89×10^{-1}	-1.36×10^{-2}	3.15	67.0	1.63	1.81	4.40×10^{-1}	0.902	1.69	6.43	1.62
4	1.57×10^{-1}	-4.31×10^{-3}	3.21	40.8	1.64	1.89	1.65×10^{-1}	0.866	3.45	1.10×10^{1}	3.65
10	7.94×10^{-2}	2.14×10^{-3}	3.26	29.4	1.66	2.05	5.24×10^{-2}	0.813	5.37	-1.11×10^{1}	7.27
40	1.54×10^{-2}	1.24×10^{-2}	3.34	17.9	1.74	2.32	2.70×10^{-3}	0.752	9.69	-3.68×10^{-1}	−7.53
100	3.16×10^{-3}	1.95×10^{-2}	3.42	12.9	1.82	2.70	1.42×10^{-4}	0.674	14.1	-4.65×10^{-2}	−1.02
					$X = 0.134$						
1	3.41×10^{-1}	-1.18×10^{-2}	1.56	82.1	1.60	1.78	3.49×10^{-1}	0.896	1.44	9.12	1.45
4	2.35×10^{-1}	-3.59×10^{-3}	1.64	51.9	1.61	1.95	2.12×10^{-1}	0.828	2.56	2.05×10^{1}	2.95
10	1.51×10^{-1}	1.96×10^{-3}	1.71	38.3	1.63	2.07	1.07×10^{-1}	0.788	3.84	-2.41×10^{1}	5.10
40	4.95×10^{-2}	1.06×10^{2}	1.84	24.2	1.71	2.41	1.64×10^{-2}	0.709	6.95	−1.44	32.0
100	1.61×10^{-2}	1.64×10^{2}	1.96	17.9	1.86	2.80	2.22×10^{-3}	0.665	10.4	-2.93×10^{-1}	−6.48
					$X = 0.208$						
1	4.27×10^{-1}	-1.11×10^{-2}	0.769	104.0	1.52	1.84	3.33×10^{-1}	0.825	1.10	1.28×10^{1}	1.23
4	3.75×10^{-1}	-4.19×10^{-3}	0.841	67.9	1.53	2.02	3.26×10^{-1}	0.758	1.70	2.98×10^{1}	2.17
10	3.10×10^{-1}	4.31×10^{-4}	0.908	51.2	1.56	2.15	2.74×10^{-1}	0.724	2.39	-2.40×10^{2}	3.31
40	1.75×10^{-1}	7.50×10^{-3}	1.035	33.4	1.62	2.49	1.26×10^{-1}	0.651	4.31	−7.61	7.61
100	9.13×10^{-2}	1.22×10^{-2}	1.163	25.2	1.89	2.81	4.50×10^{-2}	0.672	7.18	−2.37	18.4

TABLE 1. Data on fluid parameters of normal ^{3}He–^{4}He liquid mixtures

2.2. *The onset of convection*

The application of a subcritical vertical heat current to an experimental cell with the geometry described in §2.1 leads to the establishment of opposing vertical thermal and concentration gradients ∇T and ∇c across the cell, linked by the relation $\nabla c = -(k_T/T)\nabla T$ (which arises from a zero mass flux, $\boldsymbol{i} = 0$, normal to the horizontal boundaries). Provided the direction of the heat flux and the relative magnitudes of the fluid parameters are favourable, a linear marginal-state analysis using (5)–(7) predicts the existence of both stationary and overstable convective states once these gradients exceed critical values. As the heat flux is increased in a given direction, the convective state first realized is the one with the smallest critical Rayleigh number.

A calculation of the critical Rayleigh number for both stationary and oscillatory convection was first carried out by Hurle & Jakeman (1969, 1971) using a variational approach which demonstrated the existence of a branch of the solution corresponding to negative Rayleigh numbers. Subsequently Schechter *et al.* (1972) carried out an exact calculation for stationary convection, although the negative branch was omitted. Both of these sets of calculations apply to the two-component model where k_T is non-zero but A is assumed negligible. However, even if A is not negligible so that the full Soret–Dufour problem is regained, the calculations are still valid except that the dimensionless variables arising from the calculations have to be reinterpreted. Calculations of the critical Rayleigh number, both variational and exact for stationary convection and variational for oscillatory convection, have been reported by Gutkowicz-Krusin *et al.* (1979*a*, *b*) for the Soret–Dufour model. The exact solution for stationary convection in this model with the negative branch omitted was also reported independently by Lee *et al.* (1979) and the details of our approach using normal diffusive modes are given in the Appendix. In §§2.3 and 2.4 we bring together the results of all these calculations together with some further computations of our own.

2.3. *The critical Rayleigh number for stationary convection*

As shown in the Appendix, application of rigid boundary conditions to the marginal state equations for an exact solution for stationary convection yields the condition

$$f(q_0, q_1, q_2, a) + Hg(q_0, q_1, q_2) = 0, \tag{8}$$

where the functions f and g, their arguments $q_0(a,\tau)$, $q_1(a,\tau)$, $q_2(a,\tau)$ and the dimensionless wavenumber a and parameter τ are defined by (A 9)–(A 11). $H = D_T/\{D(1+A)(1+1/S)\}$ is a dimensionless variable that depends only on the thermodynamic state of the mixture. The Rayleigh number for the problem is given by

$$R = a^4\tau^3 = R_T\{(1+A)(1+S) + SD_T/D\},$$

where $R_T = gd^4\beta\beta_T/\nu D_T$, $S = -\beta_c k_T/\beta_T T$, β is the vertical temperature gradient and β_T and β_c are thermal and solutal expansion coefficients respectively. We have found it useful to define the associated Rayleigh numbers that appear to be natural to this problem,

$$\left.\begin{aligned} R_1 &= -\frac{R}{1+1/H} = \frac{gd^4\beta\beta_c k_T}{T\nu D}, \\ R_2 &= \frac{R}{1+H} = gd^4\beta\left(\beta_T - \frac{\beta_c k_T}{T}\right)\frac{1+A}{\nu D_T}, \end{aligned}\right\} \tag{9}$$

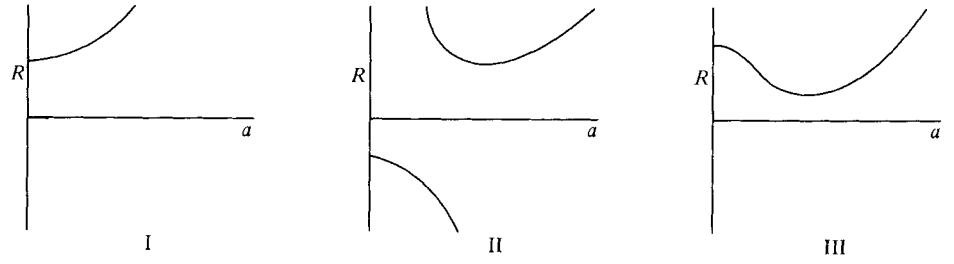

FIGURE 1. Sketch of dependence of Rayleigh number R against dimensionless wavenumber a for $H < -1$ and $H \geqslant 3.85$ (region I), $-1 \leqslant H < 0$ (region II), $0 \leqslant H < 3.85$ (region III) for stationary convection.

so that

$$R = R_2 - R_1, \quad H = -\frac{R_1}{R_2}.$$

For any given value of H the roots of (8) provide pairs of values of a and τ, and hence corresponding values of the three Rayleigh numbers. The behaviour of the Rayleigh numbers as a is varied has three forms depending on the range in which H lies: $H < -1$ and $H \geqslant 3.85$ (region I), $-1 \leqslant H < 0$ (region II), or $0 \leqslant H < 3.85$ (region III). This behaviour is sketched in figure 1. The Rayleigh numbers have stationary values that fall into two groups depending on whether $a = 0$ or $a \neq 0$. The zero-a branch in region II corresponds to $\tau < 1$, and is the 'negative branch' of Gutkowicz-Krusin *et al.* (1979*a*, *b*), all other branches in all other regions corresponding to the form of (8) where $\tau > 1$.

The stationary values of R with their associated values of a represent critical values R_s and a_s for the onset of stationary convection provided $\mathrm{d}^2|R|/\mathrm{d}a^2 < 0$; hence the zero-$a$ value in region III is not in this category. The zero-a stationary values always correspond to $R_s = 720(1 + 1/H)$, $R_{1s} = -720$, $R_{2s} = 720/H$, and $a_s = 0$, as can be seen by expanding (8) for small a. The non-zero-a critical values R_s and a_s are of sufficient generality and practical importance that we have independently reworked them with the results shown in table 2. We used single precision arithmetic on a CDC Cyber 170–730 machine, which computes to 14 decimal digits.

It follows from this discussion that zero-a critical values exist in regions I and II and not in III, while non-zero-a critical values exist in regions II and III but not in I. This can be seen in figures 2 and 3, where the Rayleigh numbers and a_s are plotted respectively against H. These data are in agreement with those of Schechter *et al.* (1972) and Gutkowicz-Krusin *et al.* (1979*b*) (their R is equivalent to our R_2), are independent of the omission of the Dufour term or the term $AD\nabla^2 T$ in (6), and were used by us (Lee *et al.* 1979) in a preliminary analysis of our data.

It is worth noting that if $H = 0$ we regain the stationary one-component problem with rigid boundaries at fixed temperatures, since (8) becomes

$$f(q_0, q_1, q_2, a) = 0,$$

leading to a critical Rayleigh number of 1707.7618 and a critical wavenumber of 3.1163. If $|H|$ is large (8) becomes

$$g(q_0, q_1, q_2) = 0,$$

corresponding to the stationary one-component problem with rigid boundaries and fixed temperature gradient normal to these boundaries (Verlarde & Schechter 1972)

H	a_s	R_s	H	a_s	R_s
−0.75	5.315	4392.69	0.85	2.214	1259.07
−0.70	5.015	3831.61	0.90	2.175	1244.79
−0.65	4.761	3417.08	0.95	2.136	1231.20
−0.60	4.543	3099.23	1.00	2.099	1218.26
−0.55	4.352	2848.20	1.10	2.026	1194.15
−0.50	4.183	2645.13	1.20	1.955	1172.11
−0.45	4.031	2477.55	1.30	1.887	1151.90
−0.40	3.894	2336.96	1.40	1.822	1133.28
−0.35	3.769	2217.33	1.50	1.758	1116.06
−0.30	3.655	2114.30	1.60	1.696	1100.10
−0.25	3.549	2024.64	1.70	1.635	1085.24
−0.20	3.451	1945.88	1.80	1.575	1071.39
−0.15	3.359	1876.15	1.90	1.517	1058.42
−0.10	3.273	1813.96	2.00	1.459	1046.27
−0.05	3.193	1758.15	2.10	1.402	1034.85
0.00	3.116	1707.76	2.20	1.346	1024.10
0.05	3.044	1662.04	2.30	1.290	1013.95
0.10	2.975	1620.37	2.40	1.234	1004.36
0.15	2.910	1582.20	2.50	1.178	995.28
0.20	2.848	1547.13	2.60	1.122	986.67
0.25	2.788	1514.77	2.70	1.065	978.48
0.30	2.731	1484.82	2.80	1.008	970.70
0.35	2.675	1457.02	2.90	0.949	963.29
0.40	2.622	1431.13	3.00	0.890	956.21
0.45	2.571	1406.96	3.10	0.828	949.46
0.50	2.522	1384.35	3.20	0.764	943.00
0.55	2.474	1363.14	3.30	0.697	936.82
0.60	2.428	1343.21	3.40	0.626	930.89
0.65	2.383	1324.43	3.50	0.548	926.21
0.70	2.339	1306.71	3.60	0.460	919.75
0.75	2.296	1289.97	3.70	0.355	914.51
0.80	2.255	1274.11	3.80	0.207	909.46

TABLE 2. The dependence of the critical Rayleigh number R_s and critical wavelength a_s on the parameter H

and leading to a critical Rayleigh number of 720 and critical wavenumber of zero (Hurle, Jakeman & Pike 1967).

2.4. *The critical Rayleigh number for oscillatory convection*

Unlike the onset of stationary convection, no exact solution has been published for the onset of oscillatory convection (also termed overstability) for the Soret–Dufour problem with rigid, impermeable, constant-temperature horizontal boundaries. This corresponds to solving the marginal-state equations (A 1)–(A 3) with $\sigma \neq 0$ with the boundary conditions (A 4)–(A 6).

However, Gutkowicz–Krusin *et al.* (1979*b*, equations (14) and (15)) have provided two variational expressions for the critical Rayleigh number at the onset of overstability, one of which has been considered previously by Hurle & Jakeman (1971). The Rayleigh number R in these expressions, which we denote R_G, is equivalent to $R_{20}/(1+A)$ or $-R_{10}/H(1+A)$ in our notation, where R_{10} and R_{20} are

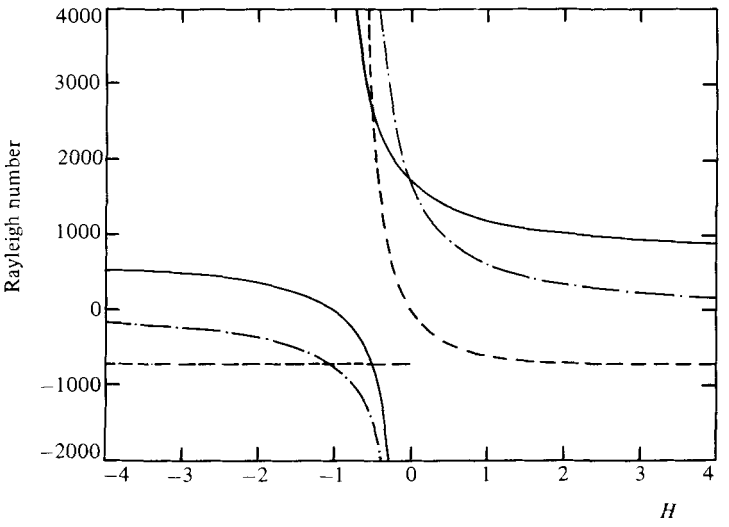

FIGURE 2. H-dependence of the critical Rayleigh numbers R_s (——), R_{s1} (– – – –) and R_{s2} (–·–·–·–·–) for stationary convection when both boundaries are rigid, perfectly conducting and impermeable, including both the zero-a_s branch and the non-zero-a_s branch.

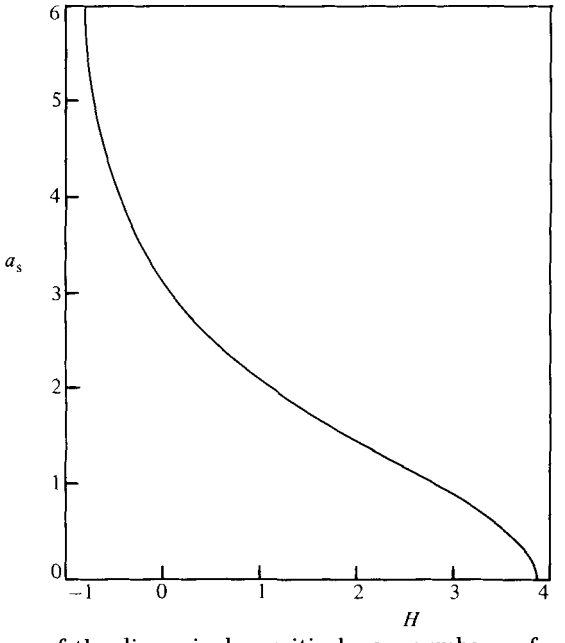

FIGURE 3. H-dependence of the dimensionless critical wavenumber a_s for stationary convection when both boundaries are rigid, perfectly conducting and impermeable. Outside the range $0 \leqslant H < 3.85$ another branch exists for which a_s is zero.

critical values of R_1 and R_2 respectively for the onset of overstability. The integrals in the expressions are approximations for ease of computation in that only the first term in a Fourier expansion of the temperature perturbation is retained. As in the case of stationary convection, Gutkowicz-Krusin *et al.* (1979*b*) found that even modes produced lower critical Rayleigh numbers than odd modes. In contrast with the onset

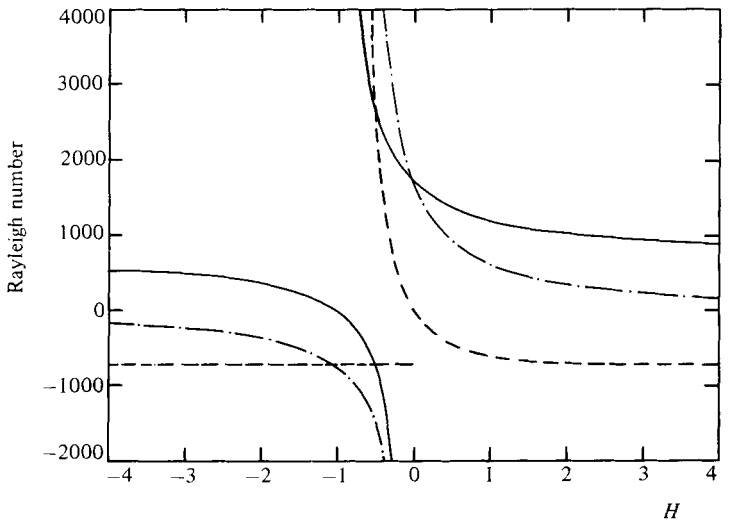

FIGURE 2. H-dependence of the critical Rayleigh numbers R_s (——), R_{s1} (– – – –) and R_{s2} (–·–·–·–·–) for stationary convection when both boundaries are rigid, perfectly conducting and impermeable, including both the zero-a_s branch and the non-zero-a_s branch.

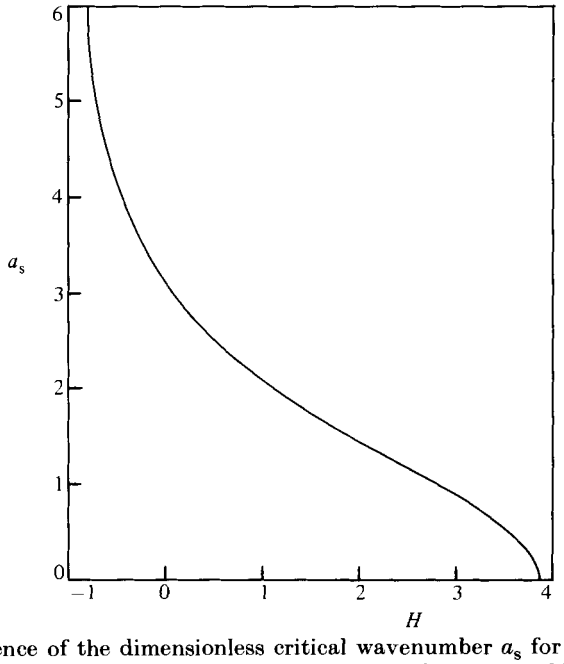

FIGURE 3. H-dependence of the dimensionless critical wavenumber a_s for stationary convection when both boundaries are rigid, perfectly conducting and impermeable. Outside the range $0 \leqslant H < 3.85$ another branch exists for which a_s is zero.

critical values of R_1 and R_2 respectively for the onset of overstability. The integrals in the expressions are approximations for ease of computation in that only the first term in a Fourier expansion of the temperature perturbation is retained. As in the case of stationary convection, Gutkowicz-Krusin *et al.* (1979*b*) found that even modes produced lower critical Rayleigh numbers than odd modes. In contrast with the onset

LLT	GCR	LLT	GCR
c	x_1	$D_T k_T/T$	α_2
T	T	ATD/k_T	$\beta_1 = \gamma_1$
D	D	S	S
D_T	k	A	$\gamma_1\gamma_2/D^2$
κ	λ	$(1+A)^{-1}$	D/β_2
β_T	α	H	ψ
β_c	$-\beta$	R_2	$\tilde{R}$
DK_T/T	γ_2	Sc'	Sc

TABLE 3. Comparison of notation used by us (LLT) and Gutkowicz-Krusin *et al.* (1981) (GCR)

$$R_T = \frac{gd^4\beta\beta_T}{\nu D_T}, \quad R_1 = -R_T\frac{SD_T}{D}$$
$$R_2 = R_T(1+A)(1+S), \quad R = R_2 - R_1$$

R_S, R_{1S}, R_{SS} — Theoretical values of R, R_1 and R_2 at the onset of stationary convection

R_0, R_{10}, R_{20} — Theoretical values of R, R_1 and R_2 at the onset of oscillatory convection

$R_G = R_{20}/(1+A)$

$R_{1\,crit}$ = experimentally determined value of R_1 at the onset of convection

TABLE 4. Rayleigh-number definitions used in this paper.

of stationary convection, the critical Rayleigh number depends not only on H, but also on the Prandtl number $Pr = \nu/D_T$, a modified Schmidt number $Sc' = \nu/D(1+A)$ and A. Table 3 lists the correspondence between our notation and that of Gutkowicz–Krusin *et al.* (1979*a*, *b*). Table 4 lists the definition of the different Rayleigh numbers used in this report. Note that the Prandtl number used by these authors should have the above definition, rather than $\nu/\kappa(1-\gamma_1\gamma_2/\kappa D)$ in their notation, this latter arising from their omission of the term $AD\nabla^2 T$ in their version of our equation (6).

The computed data provided by Gutkowicz-Krusin *et al.* (1979*b*) hardly covered the range of our experiments, which was not surprising in view of the dependence on four separate parameters. Consequently we made independent computations using their equations (14)–(17) for even modes in their approximation again using the Cyber 170-730 and single-precision arithmetic. Initially we attempted to reproduce the results of their figure 7, and obtained agreement to within 5 % using their expression (15), the smallest discrepancy occurring for the four lower curves and the largest for the case $Pr = \frac{2}{3}$, $Sc = \frac{5}{6}$, $D/\beta_2 = \frac{4}{5}$ in their notation. We had no success with their expression (14), which generated discontinuous values of R_G as H was varied, even using double-precision arithmetic, and we are still in correspondence with these authors on this point. Finally we used their expression (15), but with values for the four parameters appropriate to our experiments and derived from data such as those in table 1. The results of this last calculation are listed in table 5 and discussed further in §4.2.

$T-T_A$ (mK)	ΔT_C (mK)	Pr	$(1+A)^{-1}$	Sc'	H	$R_{1\,crit}$	R_{10}	ω_0	a_0
					$X = 0.016$				
2.41	−0.066	0.602	0.63233	2.95	4.00	-3.90×10^{3}	—	—	—
3.61	−0.197	0.618	0.75820	4.17	5.60	-9.73×10^{3}	—	—	—
4.82	−0.403	0.626	0.83755	5.19	7.10	-1.69×10^{4}	—	—	—
7.26	−0.550	0.633	0.92158	6.77	1.04×10^{1}	-1.71×10^{4}	—	—	—
11.8	4.71	0.632	0.97456	8.77	2.87×10^{1}	9.22×10^{4}	9.16×10^{5}	2.08×10^{2}	6.17
12.1	3.46	0.631	0.97616	8.88	3.24×10^{1}	6.59×10^{4}	4.66×10^{5}	1.39×10^{2}	5.31
12.6	2.76	0.630	0.97834	9.05	4.07×10^{1}	5.05×10^{4}	2.33×10^{5}	9.01×10^{1}	4.52
15.5	2.60	0.626	0.98794	9.99	-5.95×10^{1}	3.72×10^{4}	4.32×10^{4}	3.07×10^{1}	3.38
15.8	2.02	0.626	0.98867	10.08	-4.61×10^{1}	2.82×10^{4}	3.91×10^{4}	2.89×10^{1}	3.35
18.7	1.40	0.622	0.99321	10.89	-1.46×10^{1}	1.58×10^{4}	2.03×10^{4}	1.94×10^{1}	3.21
25.0	1.00	0.613	0.99742	12.42	−5.11	7.39×10^{3}	8.59×10^{3}	1.16×10^{1}	3.12
37.2	0.687	0.601	0.99943	14.87	−1.77	2.62×10^{3}	3.15×10^{3}	6.28	3.09
63.4	0.465	0.571	0.99995	18.83	-4.72×10^{-1}	6.16×10^{2}	8.42×10^{2}	2.80	3.08
91.1	0.447	0.561	0.99999	22.48	-1.82×10^{-1}	2.51×10^{2}	3.22×10^{2}	1.52	3.08
					$X = 0.079$				
2.39	−0.035	0.879	0.79271	2.64	2.67	-2.48×10^{3}	—	—	—
4.97	−0.243	0.858	0.88430	3.86	4.21	-1.79×10^{4}	—	—	—
9.99	−0.403	0.813	0.95019	5.38	7.26	-1.79×10^{4}	—	—	—
15.0	−0.898	0.808	0.97505	6.45	1.17×10^{1}	-3.06×10^{4}	—	—	—
23.6	4.47	0.782	0.99000	7.80	8.90×10^{1}	1.05×10^{5}	6.91×10^{4}	4.48×10^{1}	3.77
24.3	5.16	0.780	0.99064	7.90	1.87×10^{2}	1.18×10^{5}	5.88×10^{4}	4.03×10^{1}	3.67
24.7	3.89	0.779	0.99096	7.95	4.70×10^{2}	8.73×10^{4}	5.42×10^{4}	3.82×10^{1}	3.62
25.7	3.68	0.776	0.99175	8.08	-1.59×10^{2}	7.94×10^{4}	4.50×10^{4}	3.39×10^{1}	3.52
25.7	3.58	0.776	0.99175	8.08	-1.59×10^{2}	7.73×10^{4}	4.50×10^{4}	3.39×10^{1}	3.52
26.4	3.94	0.774	0.99225	8.17	-8.26×10^{1}	8.28×10^{4}	4.02×10^{4}	3.15×10^{1}	3.47
31.1	2.20	0.766	0.99478	8.75	-1.93×10^{1}	3.91×10^{4}	2.28×10^{4}	2.20×10^{1}	3.28
36.4	1.57	0.758	0.99652	9.34	-1.01×10^{1}	2.34×10^{4}	1.49×10^{4}	1.68×10^{1}	3.20
41.8	1.26	0.748	0.99761	9.89	−6.67	1.60×10^{4}	1.07×10^{4}	1.38×10^{1}	3.15
50.4	1.03	0.724	0.99860	10.52	−4.20	1.04×10^{4}	7.18×10^{3}	1.09×10^{1}	3.12
73.1	0.736	0.696	0.99957	12.33	−1.92	4.35×10^{3}	3.43×10^{3}	6.87	3.09
96.3	0.566	0.677	0.99984	13.91	−1.10	2.13×10^{3}	1.99×10^{3}	4.88	3.08
					$X = 0.134$				
0.173	−0.017	0.999	0.67947	0.722	6.26×10^{-1}	-8.99×10^{2}	—	—	—
0.345	−0.028	0.960	0.70922	0.963	8.79×10^{-1}	-1.75×10^{3}	—	—	—
0.525	−0.064	0.936	0.72084	1.13	1.07	-4.27×10^{3}	—	—	—

0.701	−0.078	0.917	0.73027	1.26	1.23	-5.49×10^3	—	—	—
0.875	−0.053	0.904	0.73715	1.37	1.36	-3.85×10^3	—	—	—
1.73	−0.204	0.866	0.76697	1.78	1.89	-1.61×10^4	—	—	—
2.59	−0.272	0.846	0.79262	2.12	2.34	-2.20×10^4	—	—	—
3.46	−0.369	0.834	0.81410	2.40	2.73	-2.98×10^4	—	—	—
4.34	−0.234	0.824	0.83192	2.65	3.09	-1.86×10^4	—	—	—
8.72	−0.591	0.792	0.89169	3.62	4.67	-4.21×10^4	—	—	—
13.0	−0.658	0.776	0.92470	4.32	6.11	-4.15×10^4	—	—	—
17.5	−0.862	0.757	0.94501	4.91	7.80	-4.81×10^4	—	—	—
22.0	−0.882	0.742	0.95883	5.42	9.77	-4.39×10^4	—	—	—
26.3	−1.08	0.731	0.96801	5.83	1.22×10^1	-4.87×10^4	—	—	—
30.8	−0.970	0.725	0.97490	6.24	1.57×10^1	-3.93×10^4	—	—	—
35.8	5.85	0.714	0.98035	6.63	2.20×10^1	2.14×10^5	4.04×10^5	1.49×10^2	5.55
37.6	4.76	0.710	0.98195	6.67	2.51×10^1	1.65×10^5	2.38×10^5	1.07×10^2	4.92
39.4	3.95	0.709	0.98340	6.86	2.99×10^1	1.33×10^5	1.64×10^5	8.40×10^1	4.50
39.6	3.81	0.709	0.98356	6.88	3.06×10^1	1.29×10^5	1.58×10^5	8.20×10^1	4.46
42.4	3.04	0.704	0.98543	7.10	4.28×10^1	9.75×10^4	1.03×10^5	6.18×10^1	4.05
44.2	2.69	0.701	0.98651	7.22	5.70×10^1	8.35×10^4	8.34×10^4	5.36×10^1	3.88
47.0	2.29	0.697	0.98798	7.41	1.15×10^2	6.73×10^4	6.40×10^4	4.49×10^1	3.69
50.6	1.71	0.712	0.98959	7.84	-4.02×10^2	4.59×10^4	4.94×10^4	3.71×10^1	3.54
51.3	1.83	0.710	0.98986	7.88	-2.16×10^2	4.87×10^4	4.72×10^4	3.60×10^1	3.52
55.3	1.45	0.704	0.99124	8.13	-6.01×10^1	3.60×10^4	3.76×10^4	31.0	3.42
65.1	1.10	0.693	0.99378	8.70	-2.17×10^1	2.32×10^4	2.47×10^4	23.6	3.28
70.7	1.01	0.689	0.99486	9.01	-1.58×10^1	1.96×10^4	2.05×10^4	21.0	3.24
90.5	0.756	0.673	0.99713	9.99	−8.06	1.12×10^4	1.26×10^4	15.4	3.16
					$X = 0.208$				
55.5	6.64	0.691	0.91458	5.46	9.85	5.12×10^5	—	—	—
59.2	4.81	0.690	0.91997	5.62	1.04×10^1	3.60×10^5	—	—	—
61.0	4.01	0.688	0.92225	5.70	1.07×10^1	2.95×10^5	—	—	—
63.0	3.65	0.687	0.92459	5.79	1.10×10^1	2.65×10^5	—	—	—
64.8	3.11	0.686	0.92658	5.86	1.13×10^1	2.22×10^5	—	—	—
65.7	3.00	0.685	0.92748	5.90	1.14×10^1	2.13×10^5	—	—	—
73.5	2.11	0.682	0.93629	6.22	1.27×10^1	1.41×10^5	—	—	—
83.1	1.50	0.678	0.94451	6.58	1.45×10^1	9.32×10^4	—	—	—
100.0	1.20	0.672	0.95692	7.16	1.84×10^1	6.65×10^4	—	—	—

TABLE 5. Experimental data on the onset of convection

3. Experiments on liquid ^{3}He/^{4}He mixtures

3.1. *Cryostat and cell*

The RB experimental cell used for the measurements to be described is suspended inside a stainless-steel vacuum can by a rigid support of stainless steel and epoxy construction, providing good thermal isolation of the cell from the vacuum-can walls. The can is rigidly attached to the top plate of a liquid-helium cryostat via thin-wall evacuated stainless-steel tubing and is surrounded by a pumped superfluid liquid-helium bath maintained at a fixed temperature T_B between 1.4 K and 2.0 K depending on the mixture concentration in use.

The details of the cell are shown in figure 4. The volume occupied by liquid mixture is cylindrical with diameter 2.48 cm, height 0.21 cm and axis vertical, and hence has aspect ratio $\Gamma = 6.25$. The upper and lower plane horizontal boundaries are oxygen-free high-conductivity copper machined flat and subsequently polished with crocus cloth, providing isothermal surfaces. These boundaries are separated by a cylindrical cell wall of low-conductivity thin-wall (0.025 cm) stainless-steel tubing silver-brazed vacuum-tight onto the copper boundaries. The cell is filled through a small hole (0.025 cm diameter) in one of the plates from a 0.025 cm internal-diameter stainless-steel capillary tube. The end of each copper plate is machined to form a bobbin around which is wound in bifilar fashion a coil of insulated Eureka wire of diameter 0.006 cm. Each coil is varnished in position and has electrical resistance 190 Ω and is used for applying heat to the appropriate boundary. Two electrical carbon resistance thermometers are thermally anchored to each plate. This is achieved by coating each thermometer in varnish, wrapping it completely with a piece of copper foil before the varnish sets and subsequently bolting the foils to tapped holes in each plate. Further thermal contact between thermometer and plate is achieved by taking a few turns of each connecting lead around a copper post screwed into the plate just before the leads are soldered to the resistance.

The plate with the fill line is termed the 'controlled' or C-plate since its temperature is regulated at temperature T_C through an electronic temperature controller to within 10^{-6} K utilizing one of the thermometers (R_C) and the heater H_C in a negative feedback loop with a response time of 0.1 s. This plate is chosen for temperature regulation to ensure that heat transported through the fill line capillary does not contribute to convection. The heat dissipated in H_C is dumped in the helium bath via a thermal link made from a bundle of fine copper wires connected between the C-plate and the vacuum can brass top-plate. This maintains a temperature difference $T_C - T_B$ of a few tenths of a degree between cell and bath. The thermal resistance of the link is about 500 K W^{-1} at the temperature of the experiment, and with the heat capacity of the mixture (that of the cell material is negligible) provides a time constant of about 30 minutes for the cell to achieve equilibrium with the bath.

The heater H_F on the 'floating' or F-plate is used to provide the convection heat flux into the cell. The thermometer R_F on this plate whose temperature is T_F is used for calibration purposes. The thermometers R_{DF} and R_{DC} are a matched pair whose resistance ratio provides information on the temperature difference ΔT between the two boundaries. The cell is capable of being inverted so that the convection heat flux can be applied from either above or below.

Insulated Eureka wire of the same type used for the heater coil is used as electrical leads from the resistance thermometers to the leadthrough terminals on the vacuum can. Insulated superconducting Niomax wire of 0.005 cm diameter is used for connections to the heater to eliminate Joule heating and to provide a low thermal

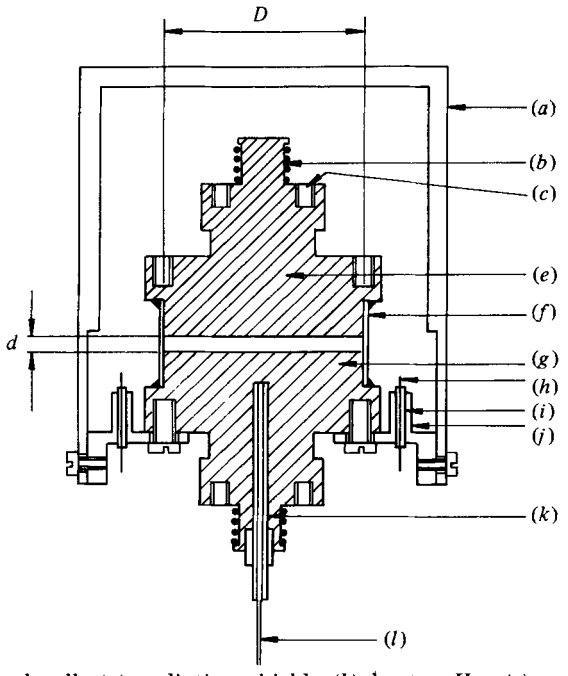

FIGURE 4. Experimental cell. (*a*) radiation shield; (*b*) heater H_F; (*c*) resistance-thermometer receptacle; (*e*) F-plate; (*f*) stainless-steel cell wall; (*g*) C-plate; (*h*) electrical leadthrough; (*i*) PTFE; (*j*) copper-post thermal anchor; (*k*) copper fill tube; (*l*) stainless-steel filling capillary; cell height $d = 2.1$ mm; cell diameter $D = 2.48$ cm. The entire cell may be inverted.

conductance path between heaters and leadthrough terminals. All electrical leads are thermally anchored at T_C at the leadthroughs by connecting each to a short piece of enamel-insulated copper wire which is wrapped round a small hollow copper post constructed as part of the C-boundary and which holds the PTFE insulated leadthrough connecting terminals. These precautions ensure that heat carried through the leads from the F-boundary is minimized since the F-boundary is only a few millikelvins above the C-boundary during an experimental run. Heat transport through radiation into the F-plate is also minimized by surrounding it by a copper radiation shield maintained at T_C by bolting it to the C-boundary. The F-plate is thus thermally isolated except through the sample mixture and the stainless-steel cell wall.

At the cell leadthroughs the leads are changed to lower-resistance 0.025 cm diameter Eureka wire and pass to the top of the vacuum can where they are thermally anchored to the can top-plate and then pass out of the cryostat via evacuated stainless tubes. This arrangement prevents lead resistance changes resulting from helium bath level fluctuations. The use of Eureka alloy also reduces the sensitivity of the leads resistance to temperature.

The resistance R_F and R_C are measured by separate manually balanced a.c. Wheatstone bridges capable of detecting changes of 10^{-3} Ω, which is 10 times greater than the estimated uncertainty in the leads resistance caused by temperature changes during the course of an experimental run. Consequently the leads resistance is included in the calibration of R_F and R_C. All the resistance thermometers are a few kΩ at the temperature of the experiment with sensitivities $(1/R)\,dR/dT \sim 1$ so that the temperature resolution of the bridges is 10^{-6} K.

The ratio $S = R_{DF}/(R_{DF}+R_{DC})$ is measured to 10^{-6} with an automatic self-balancing

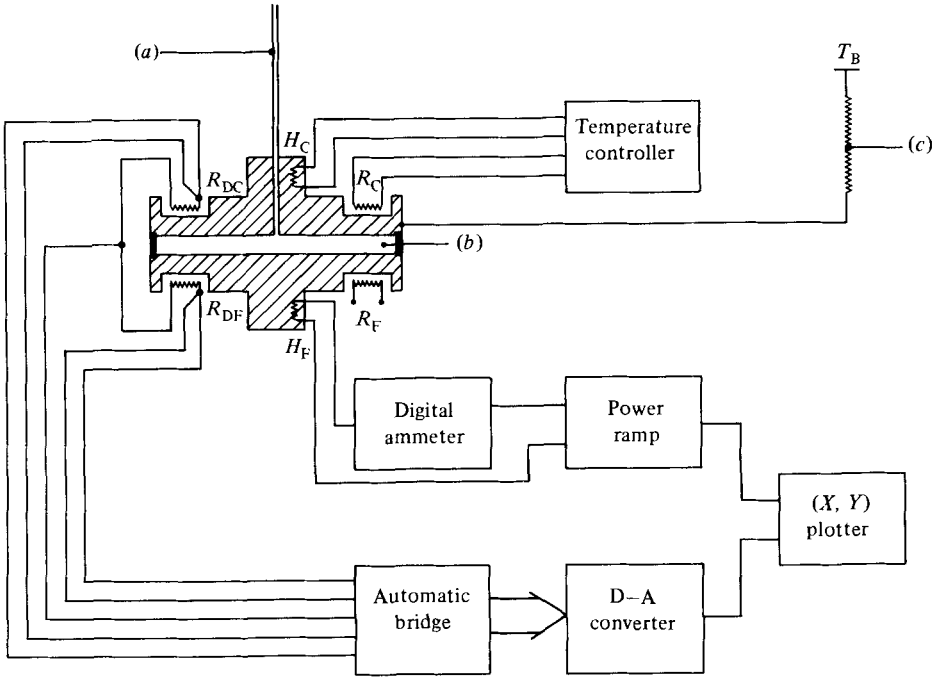

FIGURE 5. Electronics schematic showing arrangement of resistance thermometers and heaters. (*a*) cell-filling capillary; (*b*) ^{3}He–^{4}He mixture; (*c*) thermal link.

ratio-transformer bridge (Model AW7, Automatic Systems Laboratories) which has separate voltage and current leads so that leads resistance is not included, and again provides us with a resolution of about 10^{-6} K in our measurement of ΔT.

3.2. *Electronic equipment*

Most of our measurements are in the form of continuous (X, Y)-recorder plots (heating curves) of the temperature difference ΔT across the cell against the power W being dissipated in H_F. The Y-terminals of the recorder are driven by a voltage ramp linear in time which is also used as the input of an analog square-root device (Analog Devices AD534L) whose output terminals are connected across H_F. Consequently the amplitude of the original voltage ramp is proportional to the power W. The power sweeper can provide ramp rates between 0.25 μW h^{-1} and 30 μW h^{-1} and powers between 0 and 20 μW into H_F. The X-terminals of the recorder are driven by the output of a digital-to-analog converter. The input of this device is any parallel set of consecutive binary-coded decimal digits of the 6-decade automatic bridge up to a maximum of four. Normally we used the three least significant, giving the effect of an amplification by a factor of 10^3 of changes ΔS in the balance ratio of the bridge. The maximum value of ΔT ever measured (7 mK) was small enough that ΔS was always linear in ΔT to within 1 %. A block diagram of the electronic equipment is shown in figure 5.

3.3. *Mixture samples*

The ^{3}He–^{4}He gas mixtures were made by filling two known volumes with pure samples of each isotope to measured pressures and then transferring one sample out of its volume into the other volume with a Toepler pump of small dead volume. The

molar concentration of each mixture was determined to 1 % from a knowledge of the pressures and volumes. The Toepler pump was also used to pump the gas mixture into the fill line through a cold trap. The fill line passed through the pumped ^{4}He bath causing the gas to condense and fill the cell, which was cooled through the thermal link to the bath. The concentration of the liquid in the cell was measured at the start of each experimental run by measuring the λ-transition temperature of the mixture (see §3.5) and inferring the concentration from the ^{3}He–^{4}He phase diagram (Roberts & Sydoriak 1960; Gasparini & Moldover 1969), this procedure providing a precision of 0.1 % and agreeing with the less-accurate volumetric determination.

3.4. *Thermometer calibration*

The resistance thermometers R_F and R_C were calibrated between 1.8 K and 2.172 K by allowing heat exchange between the cell and the superfluid bath through low pressure ^{4}He gas in the can. Heaters H_F and H_C were not used during this procedure. The bath temperature was determined by measuring its vapour pressure with a McLeod gauge and using the 1958 ^{4}He vapour pressure tables (White 1979). The resulting calibrations were fitted to the three-parameter formula

$$\frac{1}{T} = A \ln R + \frac{B}{\ln R}$$

(White 1979) using a least-squares technique.

Calibration of the ratio S was achieved with the can and cell evacuated, holding the C-cell boundary at a fixed temperature T_C and supplying a variable power to H_F. The resulting ΔT was determined from measurements of T_C and T_F through the previous calibration and tabulated against the measured $\Delta S = S - S_0$, where S_0 is the value of S with the cell at T_C and zero heat from H_F. S_0 was found to be linear in T and ΔS proportional to ΔT, and were fitted using standard linear regression formulae.

3.5. *Experiments*

All the experimental work described here was performed near the λ-transition to take advantage of the unusual changes in the mixture parameters described in § 1. The behaviour of these parameters depends critically on the temperature difference $t = T - T_\lambda$. Consequently it was judged essential to redetermine the λ-transition of the mixture prior to each experimental run with the can evacuated. This was achieved by successively noting the values of S corresponding to zero power (S_A) and 10 μW of power (S_B) from H_F with the cell C-boundary temperature regulator set at a particular value of R_C. The value $R_{C\lambda}$ at which the fluid nearest the F-boundary first goes superfluid could then be determined from the cusp in a plot of $S_B - S_A$ against R_C, this method relying on the cusp in the thermal conductivity of a mixture at T_λ (Ahlers 1970). The absence of a cusp in a plot of S_A against R_C was evidence that unknown heat leaks into H_F were no larger than 0.1 μW.

After the λ-point location, the C-boundary controller was reset to a value R_C corresponding to the desired value of $R_{C\lambda} - R_C$ and heating curves were plotted as described in §3.2. For those heating curves where at the start of the ramp the power was zero and the bridge ratio was S_0 there was initially a region where $S - S_0$ increased in proportion to W. In many cases above some critical power W_C the gradient became abruptly smaller, and for $W > W_C$ the curve exhibited either a new linear region or a region where thermal oscillations of period of order 20 minutes were superimposed

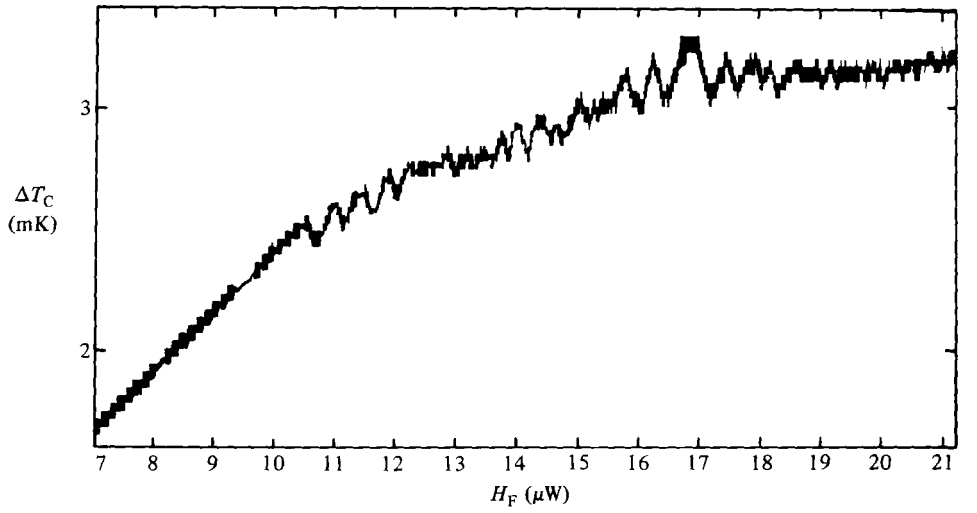

FIGURE 6. Heating curve. The steps in the curve are instrumental and associated with the self-balancing mechanism of the automatic bridge.

on an average increase of ΔS with W. Figure 6 shows a typical heating curve of this latter type.

Exploratory work on heating rates showed that W_C was smaller when the power was decreased through W_C than when it was increased. The difference between these two determinations of W_C diminished with heating rate, and was less than 5 % of W_C when the heating rate was reduced to 1 μW hour^{-1}. Consequently most of our heating curves were plotted at this heating rate.

Any heating curve showing the features described above provides information on the Rayleigh number at the convection onset from the temperature difference at which the change in gradient occurs. We obtained heating curves over a range of temperatures corresponding to $0 < t < 150$ mK and for the four molar concentrations $X = 0.016$, 0.079, 0.134 and 0.208, and (except for $X = 0.208$) both with the heat applied from below ($\beta > 0$) and from above ($\beta < 0$).

3.6. *Experimental results on the onset of convection*

Our results are summarized in figure 7 and table 5, which shows the dependence on $t = T - T_\lambda$ of the critical temperature difference ΔT_C across the cell at the point of occurrence of the change in heating curve gradient. All the data have been recalculated from the heating curves since our preliminary publication (Lee *et al.* 1979).

When heating from below, $\beta > 0$, we find that for each concentration ΔT_C is small for large t, becoming larger as t is reduced towards a value t_v where ΔT_C appears to diverge, t_v increasing with concentration. For $t < t_v$ no change in gradient occurs up to $\Delta T = 10$ mK. For $t > t_v$ and ΔT_C greater than about 1 mK the convection state shows time dependence, with oscillations in the heating curve of the order of 0.1 mK amplitude and period of order 20 minutes. Oscillations of irregular shape were maintained for over two hours if the power ramp was stopped just after the change in gradient had occurred. The frequencies were not investigated systematically, but, for comparison, in the oscillatory regime the mass and thermal relaxation times d^2/D and d^2/D_T are of order 30 minutes and 2.5 minutes respectively. For ΔT_C less than about 1 mK the convection state appears to be stationary although oscillations with

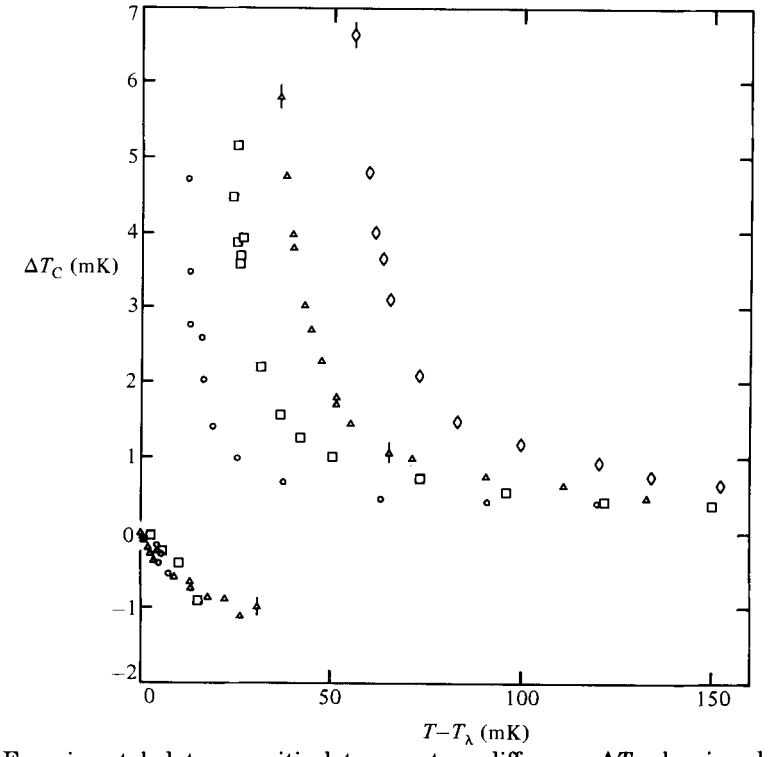

FIGURE 7. Experimental data on critical temperature difference ΔT_C showing dependence on temperature difference $T-T_\lambda$ and ^{3}He molar concentration X. ΔT_C is positive when heating from below. Representative error bars correspond to the uncertainty in determining the position in the change of slope of the heating curves. Symbols correspond to ^{3}He molar fractions as follows: ○, 0.016; □, 0.079; △, 0.134; ◇, 0.208.

period in excess of one hour and amplitude less than 0.01 mK might not have been detected.

When heating from above, $\beta < 0$, we observed gradient changes in the heating curves without oscillations, for each of the three molar concentrations 0.016, 0.079 and 0.134. The gradient change becomes smaller as t is increased, and becomes impossible to detect when $t = t_\nu$. Above t_ν there is no clear indication of any change in heating-curve slope up to $\Delta T = 10$ mK. Below t_ν the magnitude of ΔT_C decreases as the temperature is reduced towards the λ-point. No data with $\beta < 0$ exist for molar concentration 0.208.

The parameter t was computed from the quantity $R_C - R_{C\lambda}$ using the calibration described in §3.4. Thus the mean cell temperature is assumed to be T_C rather than the mean $\frac{1}{2}(T_C + T_F)$, and raises a question as to the extent to which the fluid sample is Boussinesq. Since the properties of ^{3}He–^{4}He mixtures vary most rapidly with temperature when t is small, the smallness of the parameter $\Delta T_C/t$ is of interest. When $\beta < 0$, ΔT_C decreases as t becomes smaller, in the main because of the divergence of the mass-diffusion coefficient D, and this ensures that $\Delta T_t/t$ is never greater than about 0.1 for our measurements. When $\beta > 0$, $\Delta T_C/t$ is largest near $t = t_\nu$, where the ΔT_C data diverge, and has maximum values of 0.40, 0.19, 0.16 and 0.11 respectively for the four molar concentrations in increasing order of magnitude. For $t - t_\nu > 50$ mK, T_C/t is of order 10^{-2}, decreasing with increasing t.

4. Data reduction and comparison with theory

4.1. *Fluid parameters*

The reduction of our data to dimensionless numbers requires a knowledge of the thermodynamic parameters $\rho, C_p, \beta_c, \beta_T$ and $(\partial\Delta/\partial c)_{T,p}$, and the transport coefficients k_T, κ, η and D for liquid ^{3}He–^{4}He mixtures over the range of ^{3}He concentrations and temperatures applicable to our experiments. These 'primary' parameters are obtained from direct experiments reported in the literature where available and can be used to calculate 'secondary' parameters which include D_T and ν and the dimensionless quantities A, H and the various Rayleigh numbers. An exercise of this type has been reported for liquid ^{4}He (Barenghi, Lucas & Donnelly 1980) using least-square cubic-spline fits to the data.

For mixtures the necessity of interpolating to the concentrations used in our experiments is an additional complication. In our preliminary account of this work we fitted smooth curves manually to data selected by us as being the most reliable and performed concentration interpolation using low-order polynomial fits. Recently a reliable and comprehensive set of data on $(\partial v_M/\partial T)_{X,P}$, $(\partial v_M/\partial X)_{T,P}$, k_T, κ and D have become available to us (Gestrich & Meyer 1982; Meyer 1982, private communication; Gestrich, Walsworth & Meyer 1983), where v_M is the molar volume. Least-square cubic-spline fits have been made by us to all of these data except $(\partial v_M/\partial X)_{T,P}$ for interpolating to the concentrations and temperatures used by us. These fits replace the ones used in our earlier analysis (Lee *et al.* 1979) and have made a substantial difference to the results of the analysis. The main reasons for this are that the new data on D are an order of magnitude smaller than those deduced from the diffusion relaxation times of Ahlers & Pobell (1974) and the existence of quantitative data on k_T much further above the λ-transition than the old data of Lucas & Tyler (1977) and Tanaka & Ikushima (1978) prohibits the use of k_T as an adjustable parameter. Specific notes on the data sources used in this paper now follow.

In calculating ρ, the limiting λ-transition values of the molar-volume data of Kierstead (1976) were interpolated to our concentrations and used over the entire experimental temperature range since the variation of v_M over this range for a given concentration is less than 1 %. The numerical values used were 27.4, 27.5, 28.3 and 28.9 cm^3 mol^{-1} at molar concentrations of 0.016, 0.079, 0.134 and 0.208 respectively.

For the specific heat C_p we used the data of Gasparini & Moldover (1969) on $C_{X,s}$, the specific heat at saturated vapour pressure, since the difference between $C_{X,s}$ and $C_p(X)$ is small (Ahlers 1976) over our temperature range.

A mean value of 0.62 for β_c was used over all concentrations and temperatures. This was obtained by numerically differentiating the tabular data of Kierstead (1976) and taking a mean of the data at 1.8 K over molar concentrations between 0.05 and 0.25. This procedure is justified by the observation that β_c does not vary by more than 10 % over a temperature range of $1.5\,\mathrm{K} < T < 1.8\,\mathrm{K}$ and a molar concentration range of $0.05 < X < 0.35$ according to Kierstead's (1976) data. Just prior to submission of this paper we became aware of the calculation of $(\partial v_M/\partial X)_{T,P}$ in the critical region near the superfluid transition, by Gestrich *et al.* (1983), from molar volume data using a thermodynamic relation. These data show that the variation of β_c is still less than 10 % except within 1 mK of the λ-transition (which if included increases the total variation to 20 %). For example for a 15 % mixture we determine from the graphs of Gestrich *et al.* that β_c is 0.57 at T_λ, and 0.63 and 0.69 at temperatures of 1 mK and 100 mK above T_λ respectively. This variation is no greater than the uncertainty in many other parameters.

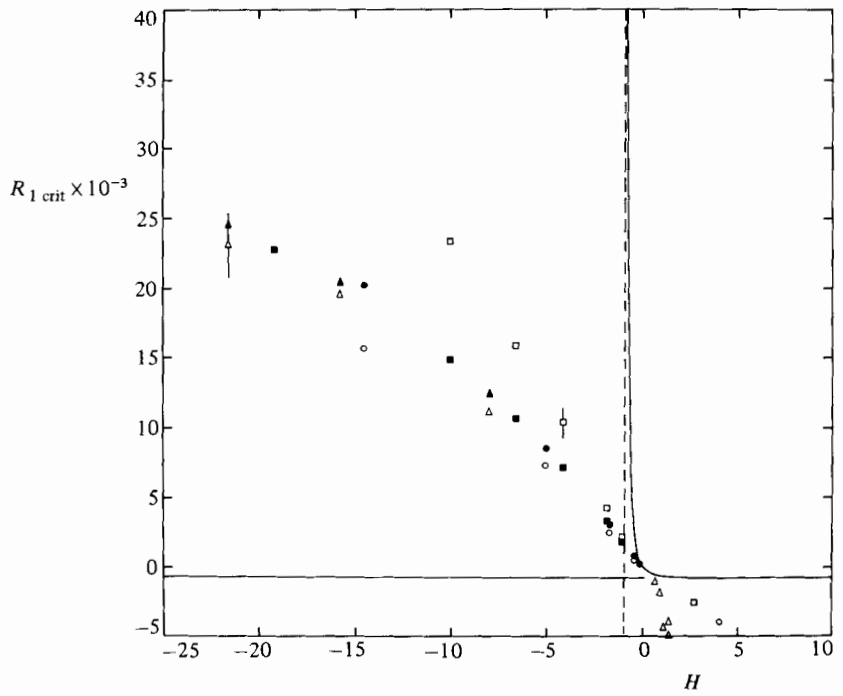

FIGURE 9. Comparison of H-dependence of experimentally derived Rayleigh numbers $R_{1\,\mathrm{crit}}$ with those derived from theory for the range $-25 \leqslant H \leqslant 10$. Symbols and error bars have the same meaning as in figure 8. The dashed line is the asymptote $H = -1$.

Gestrich *et al.* in preference to the diffusion-time-constant data of Ahlers & Pobell (1974) in view of the considerable precautions taken by the former in establishing the boundary conditions in their experimental cell and the uncertainty in converting time constants to diffusion coefficients in the latter.

4.2. *Data reduction and comparison of results with theory*

All the data on the fluid parameters, of which table 1 is a sample, were used to calculate the 'secondary' parameters discussed in §4.1 and hence to convert the experimental data on ΔT_C as functions of $T - T_\lambda$ and X to the critical value $R_{1\,\mathrm{crit}}$ of the Rayleigh number R_1 as a function of H using (9). R_1 was chosen because for stationary convection the theoretical dependence of the critical value R_{1s} on H was less complicated than either R_s or R_{2s}; in particular $R_{1s} = -720$ independent of H for the zero-a branch of solutions for $H < 0$ and $H \geqslant 3.85$. It was possible to vary H very widely during the experiments simply by adjusting the magnitude of $T - T_\lambda$ for all the concentrations used, the main reason for this being that β_T changes sign about 7 mK above T_λ and k_T is changing rapidly at this temperature so that large variations in the denominator of the third factor of the expression

$$H = \frac{D_T}{D} \frac{1}{1 + A} \frac{\beta_c k_T}{\beta_c k_T - \beta_T T},$$

are easy to achieve. The results of this conversion of the data to $R_{1\,\mathrm{crit}}$ values is displayed in table 5.

In figures 8 and 9 the experimental $R_{1\,\mathrm{crit}}$ values are compared with theory both for stationary and oscillatory convection. The solid curves correspond to stationary

convection theory and are the calculated values $R_{1s}(H)$ discussed in §2.3. The predicted Rayleigh numbers shown in figured 8 and 9 for the onset of oscillatory convection are values of $R_{10}(Pr, Sc', A, H)$ calculated as described in §2.4 with the parameters Pr, Sc', A and H corresponding to the values of $T-T_\lambda$ and X for which all the experimental data were taken. Consequently $R_{1\,\mathrm{crit}}$ and R_{10} points appear as pairs with common H-values. These calculations are also listed in table 5 together with the associated dimensionless critical frequencies ω_0 and wavenumbers a_0, and fall into two regimes. In regime I $H < 0$ and $R_G > 0$, so that the critical values R_{10}, ω_0 and a were evaluated at R_G minima. In regime II $H > 0$ and $R_G < 0$, so that in this case the critical values are evaluated at R_G maxima. However, in this second regime solutions could only be found provided $|R_{G\,\max}|$ was less than about 10^6. In both regimes where solutions existed $R_{10} > 0$.

The representative experimental errors shown in figures 7–9 correspond to the uncertainty in determining the position of the changes in slope of the heating curves. Systematic errors arising from the fluid-parameter data sources are very difficult to estimate, and we have not attempted to include them.

For all the experimentally accessible range of regime I, $-500 < H < 0$, there is reasonable agreement between experimental $R_{1\,\mathrm{crit}}$ values obtained when heating from below ($\Delta T_C > 0$, $R_{1\,\mathrm{crit}} > 0$) and the R_{10} computed data obtained using the oscillatory theory of Gutkowicz-Krusin *et al.* (1979*a*, *b*). Recall that oscillatory behaviour was always observed in the experiments in this range except when ΔT_C was less than about 1 mK (this corresponds to $-10 < H < 0$). Figure 9 shows part of this range of H in detail.

Oscillatory behaviour was also observed when heating from below ($\Delta T_C > 0$, $R_{1\,\mathrm{crit}} > 0$) in the experimentally accessible range of regime II $H_\nu < H < 500$, where H_ν is the value of H corresponding to $T-T_\lambda = t_\nu$. The agreement between the $R_{1\,\mathrm{crit}}$ data and the computed R_{10} is best for $X = 0.134$ and worst for $X = 0.016$, where in this latter case experiment and theory differ by more than the experimental error. The range of $T-T_\lambda$ used in the experiments for the concentration $X = 0.208$ turned out to be unsuitable for comparison with theory since the computed values of $-R_G$ are too large to obtain solutions.

As explained in §3.6 in the experimentally accessible range of regime II, $0 < H < H_\nu$, convection onset was only observed when heating from above ($\Delta T_C < 0$, $R_{1\,\mathrm{crit}} < 0$), and there was no sign of oscillatory behaviour. However, the experimental data for $R_{1\,\mathrm{crit}}$ lie below the computed values for stationary convection, and the difference is well outside experimental error, the data for $X = 0.016$ lying closest and that for $X = 0.208$ furthest.

5. Discussion

The reduction of our data for the onset of convection in normal liquid ^3He–^4He mixtures to the ($R_{1\,\mathrm{crit}}, H$)-plots shown in figures 8 and 9 is our best attempt at a comparison with theory given the present incomplete state of data on thermodynamic and transport parameters in these mixtures. We not that near its singularity the magnitude and sign of the parameter H is particularly sensitive to uncertainty in the parameters β_c, k_T and β_T.

Nonetheless, the agreement between theory and experiment is much better in the oscillatory region than in the stationary region. One reason for this lies in the fact that oscillatory convection is only observed when $T-T_\lambda \geqslant t_\nu$ well outside the critical region of the λ-line so that the primary parameters are varying comparatively slowly

with temperature. Consequently systematic errors in the temperature dependence of these parameters is less serious. Another reason may follow from our observation that, with heating from above, all the mixture thermal conductivities as measured from the apparently preconvecting regions of the heating curves were between 10 and 30% higher than the non-convecting data of Gestrich *et al.* (1983) interpolated to our concentrations. This was not the case when heating from below, when we obtained broad agreement with these authors. It seems plausible to us that we may have been observing a convective state transition higher than the onset when heating from above. Critical temperature differences ΔT_C corresponding to $R_{1\,\mathrm{crit}} = -720$ would be of order 10 μK, and at the time of taking our measurements our equipment was not designed to accurately examine a preconvection region where ΔT_C has the above order-of-magnitude value. Although our finite aspect ratio will increase the magnitude of the theoretical Rayleigh number for stationary convection, the calculations of Charlson & Sani (1970) show that this effect is of order 10% and much too small to account for the discrepancy between theory and experiment.

Much experimental work on the Rayleigh–Bénard instability remains to be done on normal ^{3}He–^{4}He mixtures near the λ-transition. Measurement of oscillation frequencies and the Nusselt-number–Rayleigh-number dependence near onset at various concentrations and temperatures would have special interest, since they could be compared with calculations by Gutkowicz-Krusin *et al.* (1979*a*, *b*) not utilized in this report. Good agreement with onset theory should then, we hope, stimulate further studies of finite-amplitude effects such as the first formation of layers or aperiodic behaviour.

We are grateful to Mr M. Ardron for his contribution to the computing effort and to Mr G. West for the construction of the cryogenic cell. This work was supported in part by grants from the Science and Engineering Research Council.

Appendix. Normal-mode approach to convection in mixtures

In rewriting (5)–(7) in the context of changes c' and T' in the concentration and temperature, it is natural to transform to a normal mode representation where the amplitudes of the two independent diffusive modes A and B are, in one form,

$$\chi_A = \frac{k_T}{T} T' + \left(1 - \frac{D_B}{D}\right) c',$$

$$\chi_B = \frac{k_T}{T} T' + \left(1 - \frac{D_A}{D}\right) c',$$

and where

$$D_{A,B} = \tfrac{1}{2}[D(1+A) + D_T]\left\{1 \pm \left[1 - \frac{4DD_T}{(D(1+A)+D_T)^2}\right]^{\frac{1}{2}}\right\}.$$

The expressions for χ_A and χ_B are arbitrary to the extent of multiplicative constants. Details of the transformation are given by, for example, Mountain (1965) and Lucas & Tyler (1977). While in general the amplitudes are linear combinations of c' and T', as $k_T \to 0$ (the thermohaline limit), $D_A \to D$ and $D_B \to D_T$, so that the A-mode becomes a pure mass mode with amplitude proportional to c' and the B mode a pure thermal mode with amplitude proportional to T'. Under this transformation a standard linear

stability analysis transforms (5)–(7) to the following set of equations expressed in dimensionless quantities and in the notation of Chandrasekhar (1981):

$$\left(\mathrm{D}_z^2 - a^2 - \frac{\sigma\nu}{D_A}\right) X_A = -\frac{D_B}{D_A} l W, \tag{A 1}$$

$$\left(\mathrm{D}_z^2 - \frac{\sigma\nu}{D_B}\right) X_B = -\frac{D_A}{D_B} l W, \tag{A 2}$$

$$(\mathrm{D}_z^2 - a^2 - \sigma)(\mathrm{D}_z^2 - a^2) W = \frac{g a^2 d^2 (h X_A + k X_B)}{\nu (D_A - D_B)}, \tag{A 3}$$

where

$$h = \frac{\beta_T T (D_A - D)}{k_T} + \beta_c D,$$

$$k = -\left[\frac{\beta_T T (D_B - D)}{k_T} + \beta_c D\right],$$

$$l = \frac{\beta k_T d^2}{TD},$$

and $\beta_T = -(1/\rho)\,(\partial\rho/\partial T)_{c,\,P}$ and $\beta_c = -(1/\rho)\,(\partial\rho/\partial c)_{T,\,P}$ are the thermal and solutal expansion coefficients respectively.

In these equations $X_A(z)$, $X_B(z)$ and $W(z)$ are the amplitudes of small departures from the initial values of χ_A, χ_B and u_z the vertical component of u, and have a common x, y, t dependence $\exp[\mathrm{i}(k_x x + k_y y) + pt]$. In addition the transformation has been made to dimensionless variables $a = kd$, $\sigma = pd^2/\nu$, $x \to x/d$, $y \to y/d$, $z \to z/d - \frac{1}{2}$, where $k^2 = k_x^2 + k_y^2$. Equations (A 1)–(A 3) have a structure identical with those of the linearized thermohaline problem, the difference between the two problems lying in the boundary conditions. Knobloch (1980) discusses this point in some detail.

The boundary conditions most appropriate to our experiments are those where the horizontal plates are rigid, perfectly conducting and impermeable and correspond to

$$W = \mathrm{D}_z W = 0, \tag{A 4}$$

$$(D_A - D) X_A - (D_B - D) X_B = 0, \tag{A 5}$$

$$\mathrm{D}_z (D_A X_A - D_B X_B) = 0 \tag{A 6}$$

at the plates where $z = \pm\frac{1}{2}$. Since our experiments were performed with an aspect ratio of 6.25, the effect of the sidewalls is not considered and seems justified by the analysis of Charlson & Sani (1970).

To obtain the exact solution for stationary convection one sets $\sigma = 0$ in (A 1)–(A 3) to exclude oscillatory solutions and assumes even solutions for W, X_A and X_B. Then

$$(\mathrm{D}_z^2 - a^2)^3 W = -Ra^2 W$$

defines the Rayleigh number

$$R = a^4 \mathcal{T}^3 = R_T \{(1 + A)(1 + S) + S D_T / D\}, \tag{A 7}$$

where $R_T = g d^4 \beta \beta_T / \nu D_T$ and $S = -\beta_c k_T / \beta_T T$, and application of the boundary conditions (A 4)–(A 6) yields the condition

$$f(q_0, q_1, q_2, a) + H g(q_0, q_1, q_2) = 0, \tag{A 8}$$

where

$$f(q_0, q_1, q_2, a) = \{(q_1 + q_2\sqrt{3})\sinh q_1 + (q_1\sqrt{3} - q_2)\sin q_2 - (\cosh q_1 + \cos q_2)\,F(q_0)\}\,a\tanh\tfrac{1}{2}a, \quad \text{(A 9)}$$

$$g(q_0, q_1, q_2) = (q_1^2 + q_2^2)(\cosh q_1 - \cos q_2) - \{(q_1 - q_2\sqrt{3})\sinh q_1 - (q_1\sqrt{3} + q_2)\sin q_2\}\,F(q_0) \quad \text{(A 10)}$$

and $H = D_T/\{D(1+A)(1+1/S)\}$. In the above equations

$$q_1 = \sqrt{\tfrac{1}{2}}\,a\{(1+\tfrac{1}{2}\tau) + (1+\tau+\tau^2)^{\frac{1}{2}}\}^{\frac{1}{2}}, \quad q_2 = \tfrac{1}{4}\sqrt{3}\,a^2\tau/q_1,$$
$$q_0 = a(\tau-1)^{\frac{1}{2}}, \quad F(q_0) = -q_0\tan\tfrac{1}{2}q_0 \quad (\tau \geqslant 1),$$
$$q_0 = a(1-\tau)^{\frac{1}{2}}, \quad F(q_0) = q_0\tanh\tfrac{1}{2}q_0 \quad (\tau < 1), \quad \text{(A 11)}$$

following the notation of Chandrasekhar (1961). This condition is the same as that obtained by Gutkowicz-Krusin *et al.* (1979*a*) except that their definitions of ψ (equivalent to our H) and the Rayleigh number are in error corresponding to the omission discussed in §2.1.

REFERENCES

Ahlers, G. 1970 Thermal conductivity of a ^{3}He–^{4}He mixture near the superfluid transition. *Phys. Rev. Lett.* **24**, 1333–1336.

Ahlers, G. 1975 *Fluctuations, Instabilities and Phase Transitions* (ed. T. Riste), p. 323. Plenum.

Ahlers, G. 1976 In *The Physics of Liquid and Solid Helium*, vol. 1 (ed. J. B. Ketterson and K. H. Benneman), chap. 2. Wiley.

Ahlers, G. & Pobell, F. 1974 Mass diffusivity of ^{3}He–^{4}He mixtures near the superfluid transition. *Phys. Rev. Lett.* **32**, 144–147.

Barenghi, C. F., Lucas, P. & Donnelly, R. J. 1981 Cubic spline fits to thermodynamic and transport properties of liquid ^{4}He above the λ-transition. *J. Low Temp. Phys.* **44**, 491–504.

Caldwell, D. R. 1970 Non-linear effects in a Rayleigh–Bénard experiment. *J. Fluid Mech.* **42**, 161–175.

Chandrasekhar, S. 1961 *Hydrodynamic and Hydromagnetic Stability*. Clarendon.

Charlson, G. S. & Sani, R. L. 1970 Thermoconvective instability in a bounded cylindrical fluid layer. *Intl J. Heat Mass Transfer* **13**, 1479–1496.

Da Costa, L. N., Knobloch, E. & Weiss, N. O. 1971 Oscillations in double-diffusive convection. *J. Fluid Mech.* **109**, 25–43.

De Groot, S. R. & Mazur, P. 1962 *Non-Equilibrium Thermodynamics*, chaps. 3 and 11. North-Holland.

Fetter, A. L. 1981 Onset of convection in dilute superfluid ^{3}He–^{4}He mixtures. *Physica* **107B**, 149–150. Also preprints to be published.

Gasparini, F. & Moldover, M. R. 1969 Specific heat of ^{3}He–^{4}He mixtures very near the λ-line. *Phys. Rev. Lett.* **23**, 749–752.

Gershuni, G. Z. & Zhukhovitskii, E. M. 1976 *Convective Stability of Incompressible Fluids*, chap. 7. Israel Program for Scientific Translations, Jerusalem.

Gestrich, D. & Meyer, H. 1982 Transport properties in ^{3}He–^{4}He mixtures near the superfluid transition. *Bull. Am. Phys. Soc.* **27**, 516.

Gestrich, D., Walsworth, R. & Meyer, H. 1983 Transport properties in ^{3}He–^{4}He mixtures near the superfluid transition. *Preprint.*

Gutkowicz-Krusin, D., Collins, M. A. & Ross, J. 1979*a* Rayleigh–Bénard instability in nonreactive fluids. I. Theory. *Phys. Fluids* **22**, 1443–1450.

Gutkowicz-Krusin, D., Collins, M. A. & Ross, J. 1979*b* Rayleigh–Bénard instability in nonreactive fluids. II. Results. *Phys. Fluids* **22**, 1451–1460.

HAUCKE, H., MAENO, Y., WARKENTIN, P. & WHEATLEY, J. 1981 Time-dependent thermal convection in dilute solutions of ^{3}He in superfluid ^{4}He. *J. Low Temp. Phys.* **44**, 505–533.

HUPPERT, H. E. & MOORE, D. R. 1976 Non-linear double-diffusive convection. *J. Fluid Mech.* **78**, 821–854.

HUPPERT, H. E. & MOORE, D. R. 1976 Non-linear diffusive convection. *J. Fluid Mech.* **78**, 821–854.

HURLE, D. T. J. & JAKEMAN, E. 1969 Significance of the Soret effect in the Rayleigh–Jeffreys problem. *Phys. Fluids* **12**, 2704–2705.

HURLE, D. T. J. & JAKEMAN, E. 1971 Soret-driven thermosolutal convection. *J. Fluid Mech.* **47**, 667–687.

HURLE, D. T. J., JAKEMAN, E. & PIKE, E. R. 1967 On the solution of the Bénard problem with boundaries of finite conductivity. *Proc. R. Soc. Lond.* A **296**, 469–475.

KIERSTEAD, H. A. 1976 Dielectric constant, molar volume, and phase diagram of saturated liquid ^{3}He–^{4}He mixtures. *J. Low Temp. Phys.* **24**, 497–512.

KNOBLOCH, E. 1980 Convection in binary fluids. *Phys. Fluids* **23**, 1918–1920.

LANDAU, L. D. & LIFSHITZ, E. M. 1959 *Fluid Mechanics*, chap. 6. Pergamon.

LEE, G., LUCAS, P., TYLER, A. & VAVASOUR, E. 1978 The Bénard instability in a ^{3}He–^{4}He mixture. *J. Phys. (Paris)* **41** (C6), 178–179.

LEE, G., LUCAS, P. & TYLER, A. 1979 Bénard instability measurements in ^{3}He–^{4}He mixtures near their lambda temperatures. *Phys. Lett.* **75A**, 81–84.

LUCAS, P. & TYLER, A. 1977 Thermal diffusion ratio of a ^{3}He–^{4}He mixture near its λ-transition: the onset of heat flush. *J. Low Temp. Phys.* **27**, 281–303.

MOUNTAIN, R. D. 1965 Spectral structure of critical opalescence: binary mixture. *J. Res. Natl Bur. Standards* **69A**, 523–525.

NIELD, D. A. 1967 The thermohaline Rayleigh–Jeffreys problem. *J. Fluid Mech.* **29**, 545–558.

ROBERTS, T. H. & SYDORIAK, S. J. 1960 Sound velocity, phase separation, and lambda transitions of ^{3}He–^{4}He mixtures. *Phys. Fluids* **3**, 895–902.

RYSKEWITSCH, M. G. & MEYER, H. 1979 Concentration susceptibility of ^{3}He–^{4}He mixtures near the superfluid transition. *J. Low Temp. Phys.* **35**, 103–133.

SCHECHTER, R. S., PRIGOGINE, I. & HAMM, J. R. 1972 Thermal diffusion and convective stability. *Phys. Fluids* **15**, 379–386.

SCHECHTER, R. S., VERLARDE, M. G. & PLATTEN, J. K. 1974 The two component Bénard problem. *Adv. Chem. Phys.* **26**, 265–301.

STEINBERG, V. 1981*a* Stationary convective instability in a superfluid ^{3}He–^{4}He mixture. *Phys. Rev.* **A24**, 975–987.

STEINBERG, V. 1981*b* Oscillatory convective instability in a superfluid ^{3}He–^{4}He mixture. *Phys. Rev.* **A24**, 2584–2594.

TANAKA, M. & IKUSHIMA, A. 1978 Thermal transport coefficients in ^{3}He–^{4}He mixtures near the lambda line. *Phys. Lett.* **64A**, 402–403.

TANAKA, M., IKUSHIMA, A. & KAWASAKI, K. 1977 Thermal conductivities of ^{3}He–^{4}He mixtures on the lambda line at low ^{3}He concentrations. *Phys. Lett.* **61A**, 119–121.

VERLARDE, M. G. & SCHECHTER, R. S. 1972 Thermal diffusion and convective stability. II. An analysis of the convected fluxes. *Phys. Fluids* **15**, 1707–1714.

WARKENTIN, P. A., HAUCKE, H. J., LUCAS, P. & WHEATLEY, J. C. 1980 Stationary convection in dilute solutions of ^{3}He in superfluid ^{4}He. *Proc. Natl Acad. Sci.* **77**, 6983–6987.

WEBELER, R. W. H. & ALLEN, G. 1972 Lambda-point measurements of $\eta\rho_n$ for pure ^{3}He and for three ^{3}He–^{4}He mixtures. *Phys. Rev.* **A5**, 1820–1827.

WHITE, G. K. 1979 *Experimental Techniques in Low-Temperature Physics*. Clarendon.